Inorganic Chemistry

Article

pubs.acs.org/IC

Unravelling the Proton Conduction Mechanism from Room Temperature to 553 K in a 3D Inorganic Coordination Framework

Yaxing Wang,[†,‡] Zetian Tao,[†,§,‡] Xuemiao Yin,[†,‡] Jie Shu,[∥] Lanhua Chen,[†] Daopeng Sheng,[†] Zhifang Chai,[†] Thomas E. Albrecht-Schmitt,[⊥] and Shuao Wang*[,†]

[†]School for Radiological and Interdisciplinary Sciences (RAD-X) and Collaborative Innovation Center of Radiation Medicine of Jiangsu Higher Education Institutions and [∥]Analysis and Testing Center, Soochow University, 199 Renai Road, Suzhou 215123, China

[§]Key Laboratory for Advanced Technology in Environmental Protection of Jiangsu Province, Yancheng Institute of Technology, Yancheng 224001, Jiangsu China

[⊥]Department of Chemistry and Biochemistry, Florida State University, 95 Chieftain Way, Tallahassee, Florida 32306, United States

Supporting Information

ABSTRACT: The preparation of proton-conducting materials that are functional and stable at intermediate temperatures (393−573 K) is a focal point of fuel cell development. The purely inorganic material, $HNd(IO_3)_4$, which possesses a dense 3D framework structure, can reach a maximum of 4.6×10^{-4} S·cm^{-1} at 353 K and 95% relative humidity and exhibit a high conductivity of 8.0×10^{-5} S·cm^{-1} from 373 to 553 K under the flow of wet N_2. $HNd(IO_3)_4$ exhibits a variety of improvements including high thermal stability, low solubility in water, and resistance to reducing atmosphere. The proton conductivity in such a wide temperature range originates from the intrinsic liberated protons in the structure and the resulting 1D hydrogen-bonding network confirmed by bond valence sum calculation and solid-state NMR analysis. Moreover, two different activation energies are observed in different temperature regions (0.23 eV below 373 K and 0.026 eV from 373 to 553 K), indicating that two types of proton motion are responsible for proton diffusion, as further domenstrated by temperature-dependent open-circuit voltage hysteresis in a tested fuel cell assembly as well as variable-temperature and double quantum filtered solid-state NMR measurements.

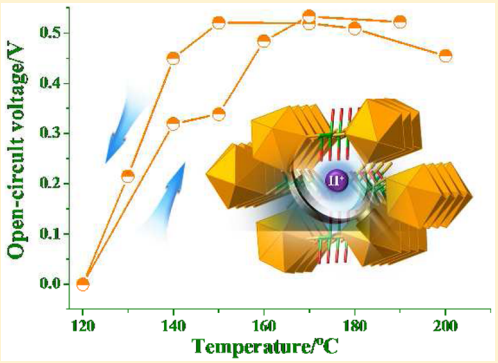

INTRODUCTION

Proton exchange membrane fuel cells (PEMFCs) with an embedded commercial Nafion (sulfonated fluoropolymer) electrolyte show great promise in portable and stationary applications.[1] Proton-conducting materials with high conductivity and fast ion transport are key components for advanced development in fuel cells system. Although Nafion can reach a high conductivity of 0.1 S cm^{-1}, the limitation on its operating conditions is a clear disadvantage and significantly restricts its wider applications. Typically, PMEFCs with a Nafion electrolyte show excellent performance below 80 °C and under a high relative humidity of 98%; however, its conductivity drops dramatically above that temperature because of dehydration. Platinum catalysts that cause hydrogen dissociation are a potential alternative under relatively low operation temperatures; however, these are largely cost prohibitive. Moreover, facile CO poisoning of platinum catalysts is promoted at low temperature when PMEFCs are equipped with methanol or methane fuels.[2] As a consequence, many attempts have been made to develop proton-conducting materials featured with high proton conductivity and robustness that can operate in low humidity or at intermediate temperatures (393−573 K) to further increase the efficiency of fuel cells.[3] Among these, high thermal stability phosphoric acid-doped polybenzimidazole shows proton conductivity higher than the order of magnitude of 10^{-2} S cm^{-1} with elevated temperature originated from enhanced mobile carrier acid groups; however, cell performance significantly deteriorated due to acid leaching in long-term operation conditions.[4] Other proposed "superprotonic" solid acids, i.e., water-soluble $CsHSO_4$ and CsH_2PO_4, also exhibit remarkable electrochemical performance in the intermediate-temperature region under a low humidity environment, but both are facing long-term stability issues owing to chemical reduction and dehydration, respectively.[5]

Recently, porous materials, especially crystalline materials such as coordination polymers (CPs) or metal organic frameworks (MOFs), have been intensively investigated in separation,[6] catalysis,[7] sensing,[8] guest delivering[9] originated from their various architectures, porous properties, designable structure, and tunable functionalities. Meanwhile, featuring good thermal stability and tunable pore for accommodation of

Received: August 7, 2015
Published: October 7, 2015

DOI: 10.1021/acs.inorgchem.5b01801
Inorg. Chem. 2015, 54, 10023−10029

versatile guest molecules, CPs/MOFs have rapidly emerged as new candidates for robust solid electrolytes in fuel cells.[10] Although practical applications are limited at the current stage, the emergence of crystalline proton conduction CPs/MOFs sheds light on better understanding of the proton transportation pathways and mechanisms at the molecular level.[11] More importantly, desired structure design and optimization is facile to achieve further enhancement of the performance. Proton-conducting CPs/MOFs are generally classified based on two different operating temperature regions. The majority of materials are operated in water-mediated environment below 373 K,[12] which is identical to other well-developed water-dependent materials, such as Nafion, α-$Zr(HPO_4)_2{\cdot}H_2O$, heteropolyacids, and so on. Only a small portion of investigations aimed to develop anhydrous proton-conducting CPs/MOFs operated in dry/wet gas (H_2, N_2, and air) in the range of 373−573 K,[13] which have better practical significance. Unlike those materials overwhelmingly depending on relative humidity, anhydrous proton-conducting CPs/MOFs exhibit high conductivity at a magnitude ranging from 10^{-5} to 10^{-3} S cm^{-1}, partially originated from (1) high diffusion of hydrogen ions through an intrinsic hydrogen-bond network,[13b−d] (2) enhanced proton conductivity when protonated guest molecules were loaded in void space of CPs/MOFs,[13a,g,i] and (3) fast proton transportation supervened with an inherent dehydration process.[13h]

While most proton-conducting CPs/MOFs materials as well as Nafion and other solid-state proton-conducting materials were operated in water, few are done under an anhydrous environment; even fewer works have investigated coordination polymers operated in both regions.[12j] Herein, we prepared a new coordination framework $HNd(IO_3)_4$ which merges the structural stability and high proton conductivity in an extremely wide operating temperature region. This crystalline compound exhibits a high conductivity at a magnitude of 8×10^{-5} S cm^{-1} in intermediate temperature from 373 to 553 K in wet N_2 and a moderate value of 4.57×10^{-4} S cm^{-1} at 353 K and 95% relative humidity. Moreover, $HNd(IO_3)_4$ shows excellent resistance to reducing H_2 and CO atmosphere at the operating temperature and water. This low-cost material is facile to be synthesized, making it a promising proton-conducting material that can further be fabricated into membrane electrode assembly.

EXPERIMENTAL SECTION

Caution! *Although $HNd(IO_3)_4$ is stable in a reducing atmosphere in this work, it is noted that iodate salts are highly oxidative and explosive when mixed with reducing agents. A safe procedure should be performed in the experiment.*

Synthesis of $HNd(IO_3)_4$. Nd_2O_3 (33.6 mg, 0.1 mmol), H_5IO_6 (1.0257 g, 4.5 mmol), and Millipore water (50 μL) were loaded into a 10 mL autoclave. The autoclave was sealed and heated to 160 °C in a box furnace for 3 days and cooled to room temperature at a rate of 5 °C/h. The product was washed with water to remove excess iodic acid; the pale pink prismatic crystals suitable for X-ray structural analysis were collected. The diamagnetic analogue $HLa(IO_3)_4$ was prepared using the same procedure. All reagents were used as received from commercial suppliers without further purification.

Fabrication of Fuel Cell Assembly. The single fuel cells were fabricated by using $HNd(IO_3)_4$ as electrolyte and a mixture of Pt−C(20% Pt), $HNd(IO_3)_4$, and naphthalene in a 3:2:1 weight ratio as both anode and cathode electrodes. The trilayer structure was copressed under a uniaxial pressure at 300 MPa. Then the prepared cells were treated at 200 °C for 3 h to sublime naphthalene and obtain porous electrodes for gas transportation.

X-ray Crystallography. Data collection was performed on a Bruker D8-Venture diffractometer with a Turbo X-ray Source (Mo Kα radiation, λ = 0.71073 Å) adopting the direct-drive rotating anode technique and a CMOS detector at room temperature. The data frames were collected using the program APEX2 and processed using the program SAINT routine in APEX2. The structures were solved by direct methods and refined by the full-matrix least-squares on F^2 using the SHELXTL-97 program.[14] All non-hydrogen atoms were refined with anisotropic displacement parameters. Crystallographic and refinement details are summarized in Table 1.

Table 1. Crystallographic Data for $hnd(IO_3)_4$

formula	$HNd(IO_3)_4$
M_r[g mol^{-1}]	844.85
cryst syst	monoclinic
space group	$P2_1/c$
a (Å)	10.5664(7)
b (Å)	7.5350(5)
c (Å)	14.1473(9)
α	90.00
β	110.51
γ	90.00
V (Å^3)	1054.98(12)
Z	4
D_c (g cm^{-3})	5.313
μ (mm^{-1})	16.687
F (000)	1472.0
T (K)	273
GOF on F^2	0.853
R_1,[a] wR_2[b] ($I > 2\sigma(I)$)	0.0190, 0.0938
R_1,[a] wR_2[b] (all data)	0.0218, 0.0968

[a] $R_1 = \Sigma||F_o| - |F_c||/\Sigma|F_o|$. [b] $wR_2 = [\Sigma w(F_o^2 - F_c^2)^2/\Sigma w(F_o^2)^2]^{1/2}$.

Solid-State NMR Measurement. Solid-state NMR experiments were performed on a sample of diamagnetic analogue of $HNd(IO_3)_4$ and $HLa(IO_3)_4$ using a Bruker Avance III HD 400 spectrometer operating at a ^{1}H Larmor frequency of 400.25 MHz and equipped with a double-resonance magic-angle spinning (MAS) probe, supporting MAS rotors of 3.2 mm outer diameter. The rf-nutation frequency for ^{1}H was 78.125 kHz, corresponding to 3.2 μs for 900 pulses. 1D ^{1}H spectra with the one-pulse excitation method were acquired at a MAS frequency of 10 kHz. A 1D ^{1}H double-quantum filtered spectrum was recorded at a 18 kHz MAS frequency with a back-to-back sequence (BaBa) to excite and reconvert the DQ signals.[15] All spectra were referenced with respect to tetramethyl silane (TMS) using solid adamantane (^{1}H, 1.85 ppm) as a secondary reference.[16]

Powder X-ray Diffraction. Powder patterns were collected from 5° to 50° with a step of 0.02° using a Bruker D8 advance X-ray diffractometer with Cu Kα radiation (λ = 1.54056 Å) equipped with a Lynxeye one-dimensional detector.

Thermal Analysis. Thermalgravimetric analysis was carried out on a NETZSCH STA 449F3 instrument in the range of 30−900 °C under nitrogen flow at a heating rate of 10 °C/min.

Solid-State UV−vis−NIR Absorption Spectroscopy. The solid-state UV−vis−NIR spectra were recorded on a Craic micro-spectrophotometer. Crystals were placed on quartz slides, and data was collected after auto-set optimization.

Alternating Current Impedance Measurements. Alternating current impedance mesurements were carried out on a Solartron SI 1260 Impedance/Gain-Phase Analyzer with an applied ac voltage amplitude of 500 mV and frequency range from 4 MHz to 1 Hz. A bulk crystalline powder of $HNd(IO_3)_4$ was compressed into a pellet with 500 kg pressure, the diameter of the pellet is 3 mm, and the thickness is in the range from 1 to 2 mm. For measurement below 100 °C, the pelletized sample attached with two gold electrodes was placed in a temperature- and humidity-controlled chamber. To determine the

DOI: 10.1021/acs.inorgchem.5b01801
Inorg. Chem. 2015, 54, 10023−10029

conductivity of the sample above 100 °C, the pelletized sample was placed into a tube furnace under a constant flow of humidified N_2 (the pressure of N_2 was approximately 1 bar), whereas the silver electrodes were used due to the complexation reaction between $HNd(IO_3)_4$ and gold at elevated temperature. All temperature points were calibrated by an external thermocouple. The data were collected after the sample was equilibrated in 50 min.

RESULTS AND DISCUSSION

Structure Description. $HNd(IO_3)_4$ can be synthesized either from the periodic acid flux method or slow evaporation in concentrated acid; both are extremely proton-rich systems. Single-crystal X-ray diffraction data reveals that $HNd(IO_3)_4$ crystallizes in a monoclinic system in $P2_1/c$ space group, which is isotypical to the lanthanum analogue $HLa(IO_3)_4$.[17] The overall structure of $HNd(IO_3)_4$ is a dense three-dimensional framework, as shown in Figure 1a. The asymmetric unit

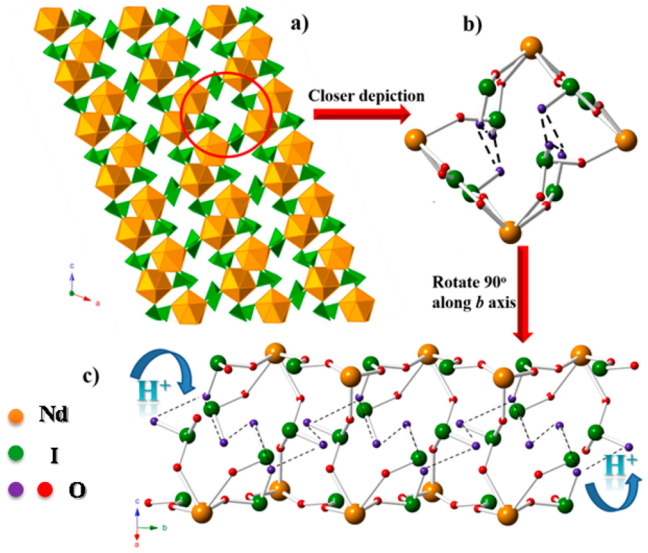

Figure 1. (a) View of the three-dimensional structure of $HNd(IO_3)_4$ along the b axis. NdO_9 polyhedra are shown in orange and IO_3 triangular pyramids in green. (b) Closer look at the partially protonated terminal oxo atoms (shown in purple) connected through H bonds shown as dashed lines. (c) Representation of 1D channels for proton diffusion along the b axis.

consists of one Nd site and four I sites. The Nd center adopts a tricapped trigonal prism geometry with nine-coordinated oxygen atoms provided by four IO_3 units. The four crystallographically independent IO_3 groups can be divided into two categories: one is η^3-IO_3 (I(2)) coordinating to three different NdO_9 polyhedra, bridging Nd centers along the b axis; the other one includes the rest of the IO_3 groups (I(1), I(3), and I(4)) with η^2-coordinating mode, with each one containing one terminal oxygen atom with the corresponding I−O bond pointing into the void space, creating 2.107 Å × 3.081 Å one-dimensional channels along the b axis, as depicted in Figure 1b.

The overall framework structure is negatively charged with a formal molecular formula of $[Nd(IO_3)_4]^-$. Considering the principle of charge balance, there has to be one positive H^+ present within the structure, most likely locating on terminal oxygen atoms forming a HIO_3 group. As shown in Table 2, BVS (bond valence sums) calculated based on the corresponding I−O bond distances for three terminal oxygen atoms are 1.33, 1.75, and 1.64, indicating that H^+ is distributed in a

Table 2. Bond Valence Sums for Terminal Oxygen Atoms and Corresponding Bond Lengths for I−O Bonds

	O(3)	O(9)	O(10)
center atom	I(1)	I(3)	I(4)
bond valence	1.33	1.75	1.64
bond length (Å)	1.894	1.793	1.817

statistical means on these oxygen atoms, where the distribution coefficients can be roughly determined by the deviation of the oxygen BVS value from 2.[18] This suggests about 50% of H^+ locates on O(3), and two sets of the rest of the 25% of H^+ bind to O(9) and O(10). The O−O distances for the neighboring terminal oxygen atoms are 3.116 (O(10)−O(9)), 2.733 (O(9)−O(3)), and 3.398 Å (O(3)−O(10)), all well within the range of hydrogen bonds. Hence, a series of proton-hopping sites is afforded along the b axis, as shown in Figure 1b. Furthermore, taking the van der Waals radii of atoms into account, the intermolecular interaction clearly exists for the terminal oxygen atoms; as illustrated in the space-filling diagram (Figure S1), the H^+ is actually confined in the narrow space of channels along the b axis rather than tightly bonding to terminal oxygen, namely, H^+ in $HNd(IO_3)_4$ is probable to diffuse effectively (Figure 1c).

Solid-State NMR Analysis. A broad peak in solid-state nuclear magnetic resonance (SSNMR) ^1H spectra of diamagnetic analogue $HLa(IO_3)_4$ clearly indicates the existence of a proton (Figure 2). Quantitatively, three peaks are

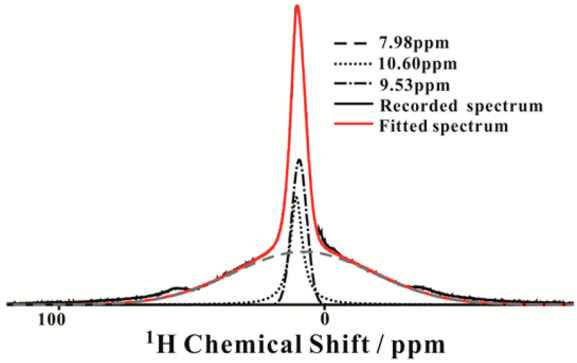

Figure 2. Line shape analysis of the SSNMR ^1H spectrum.

employed for deconvolution with resonances at 7.98, 9.53, and 10.60 ppm. The corresponding contributions are 63.9%, 19.1%, and 17.0%, respectively, highly matching the BVS calculation results, further confirming the distribution of confined H^+ on three different terminal oxygen atoms. Furthermore, two SSNMR methods are employed in this work, named one-pulse excitation and double-quantum (DQ) filtered, which, respectively, accumulate signal of full protons and the protons in a rigid system. As depicted in Figure 3, no signal is recorded using the DQ-filtered method, which implies the high local mobility of all protons in the system.

Stability Measurements. The thermal stability of the bulk sample was investigated by thermogravimetric analysis (TGA) and differential scanning calorimetry (DSC) methods under N_2 atmosphere. As indicated by the TGA curves (Figure S2), $HNd(IO_3)_4$ shows no clear weight loss until 573 K, demonstrating its high thermal stability in a wide temperature range. The DSC (Figure S3) curve further confirmed the structural integrity of bulk samples, with no clear signals until

DOI: 10.1021/acs.inorgchem.5b01801
Inorg. Chem. 2015, 54, 10023−10029

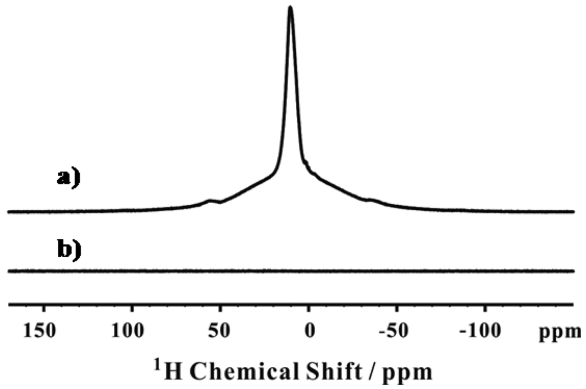

Figure 3. Solid-state NMR ^{1}H spectrum of $HLa(IO_3)_4$ using the one-pulse excitation method (a), and 1D ^{1}H double-quantum filtered spectrum (b).

573 K, indicating no phase transition in this temperature range, which is also confirmed by the variable-temperature XRD data (Figure S5). In addition, the structural stability of $HNd(IO_3)_4$ was checked under reducing H_2 and CO atmosphere at 473 K as well as by soaking the crystals in water and methanol for 3 days, where no crystal degradation was observed (Figure 4), suggesting the long-term stability of this material at fuel cell operation conditions.

Conductivity Properties. The proton conductivity of $HNd(IO_3)_4$ was evaluated by alternating current (ac) impedance spectroscopy from room temperature to 553 K. As an established measuring method, bulk crystalline powder of $HNd(IO_3)_4$ was compressed into a pellet attached with two gold/silver electrodes and placed in a temperature- and

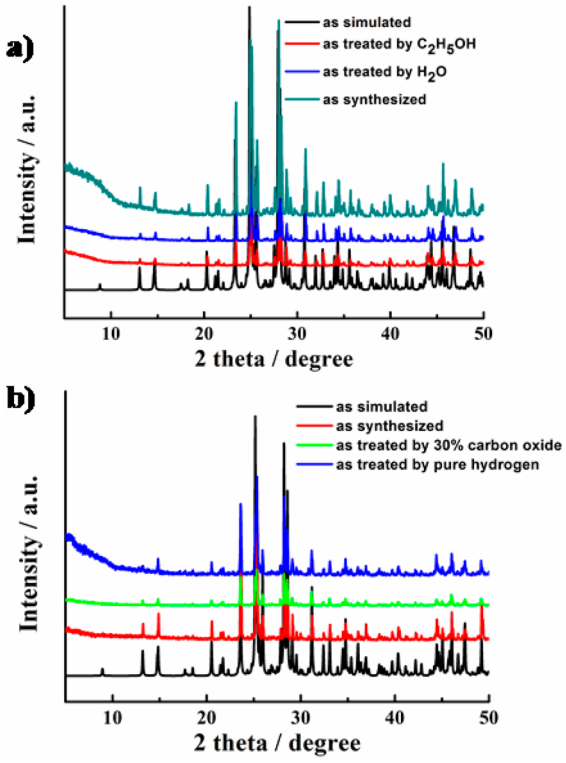

Figure 4. (a) PXRD data for $HNd(IO_3)_4$ after being soaked in H_2O or ethanol for 3 days. (b) PXRD data for $HNd(IO_3)_4$ treated by reducing atmosphere under 200 °C.

humidity-controlled chamber. At 303 K/30% RH, the conductivity of $HNd(IO_3)_4$ is quite low with a value of 8.0×10^{-9} S cm^{-1}, which is comparable with those of bulk organic molecules (e.g., imidazole), suggesting that the effective transportation of H^+ ions is limited by a strong interaction existing in the structure. However, this value is strongly humidity dependent, which further increases to 1.78×10^{-4} S cm^{-1} at 95% RH. As demonstrated in Nyquist plots (Figure 5,

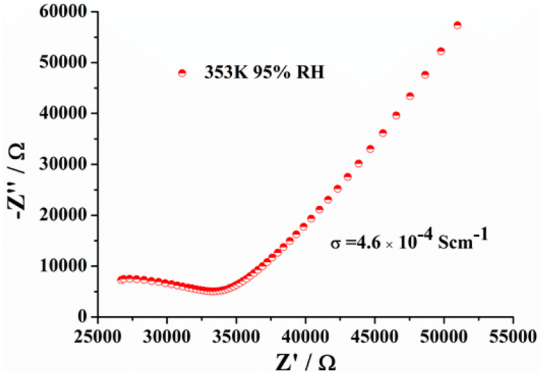

Figure 5. Nyquist plot for $HNd(IO_3)_4$ at 353 K 95% RH.

detailed results are shown in Figures S6 and S7), the conductivity is elevated with an increase of temperature, finally reaching a maximum value of 4.6×10^{-4} S cm^{-1} at 353 K and 95% RH. Similar with other extensively investigated crystalline proton-conducting materials, water plays an important role in tuning proton conductivity, implying that confined H^+ in the channel was activated by water and hence responsible for the proton conductivity. Owing to the high thermal stability, it may be a promising candidate for proton-conducting material operated in the temperature region above 373 K. The pelletized powder $HNd(IO_3)_4$ was placed in a tube furnace under a constant flow of humidified N_2 to determine the conductivity of $HNd(IO_3)_4$ above 373 K. Notably, $HNd(IO_3)_4$ held a high conductivity at a magnitude of 8.0×10^{-5} S cm^{-1} for the whole range from 373 to 553 K, as depicted in Table S1.

Activation Energy Properties and Proton Conduction Mechanism. The high proton conductivity observed in such a wide temperature range promoted us to further investigate the conduction mechanism. As shown in Figure 6a and 6b, there

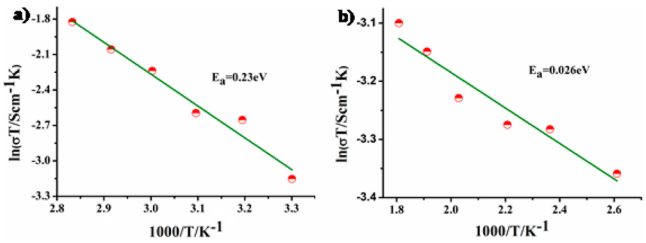

Figure 6. Arrhenius plots of $HNd(IO_3)_4$ below 373 K (a) and above 373 K (b).

are two distinguished Arrhenius plots in two separated temperature regions. The calculated activation energy value E_a is 0.23 eV below 373 K. Surprisingly, the value of E_a is 0.026 eV above 373 K, which is much lower than the former one. Considering the typical activation energy value and the humidity dependence of the conductivity below 373 K, the Grotthuss mechanism predominantly contributes to proton

DOI: 10.1021/acs.inorgchem.5b01801
Inorg. Chem. 2015, 54, 10023−10029

conduction, where conductivity carrier, proton, diffuses along the hydrogen-bond network with the aid of water. When above 373 K, thermal activation gradually plays a more important role with dramatically dropped humidity at higher temperature. Similar with other reported systems with an abnormally low activation energy (<0.1 eV),[19] the thermal activation effect on confined H^+ in proton hopping sites along the *b* axis is responsible for the diffusion, where short O−O distances enable "soft" H^+ to jump between adjacent oxygen atoms, giving rise to so-called "oscillatory proton transfer".[19] As demonstrated in Figure 7, variable-temperature SSNMR ^1H

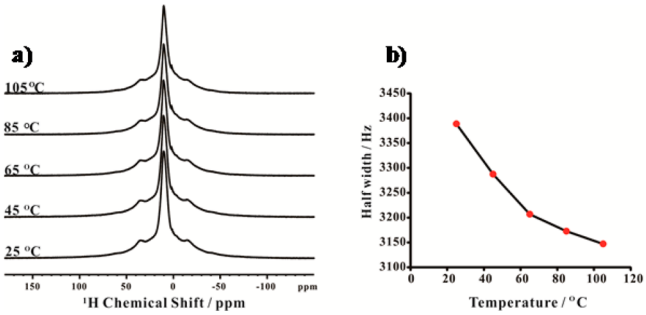

Figure 7. (a) Variable-temperature SSNMR ^1H spectra recorded from 25 to 105 °C with an increment of 20 °C. (b) ^1H peaks line width as a function of elevated temperature.

spectra are recorded from 25 to 105 °C with an increment of 20 °C. The ^1H peak line width slightly decreases from 3390 to 3140 Hz via increasing experimental temperature; the higher temperature spectrum displays a lower peak line width, clearly indicating that thermal activation results in rapid proton exchange and diffusion, therefore giving rise to much lower activation energy. Unlike reported solid acid, such as $CsHSO_4$, which undergoes a superprotonic phase transition accompanied by a transformation from an ordered to a disordered hydrogen-bond network, resulting in remarkably enhanced proton conductivity.[20] One significant feature in $HNd(IO_3)_4$ is the absence of phase transitions, while high proton conductivity in $HNd(IO_3)_4$ is originated from proton diffusion within the inherent hydrogen-bond network with the aid of water and thermal activation.

Performance of Testing Fuel Cell Assembly. Direct evidence to clarify the long-range proton conduction is to observe the performance in the tested fuel cell. A sandwich proton electrolyte assembly was fabricated by a dense $HNd(IO_3)_4$ electrolyte attached with two Pt/C electrodes. The heating and cooling cycle of electromotive force curves were measured from 120 to 200 °C, which was the ideal operating temperature region for PEMFCs. As shown in Figure 8a, the voltage of the cell at the initial temperature (~393 K) is close to zero, possibly due to the fact that the low thermal activation effect is not strong enough to overcome the energy barrier of the intermolecular interaction and hence has no effect on the transportation of confined H^+, whereas the diffusion of H^+ was activated with the elevation of temperature, resulting in a gradual enhancement of the open-circuit voltage. This thermal activation mechanism of confined H^+ was also observed in the cooling cycle. Notably, the heating and cooling steps are not superimposed with each other, establishing a hysteresis loop, which is again supportive for the thermal activation hypothesis (Figure 8a). Figure 8b presents the assembled cell tested on wet hydrogen/air at 170 and 190 °C

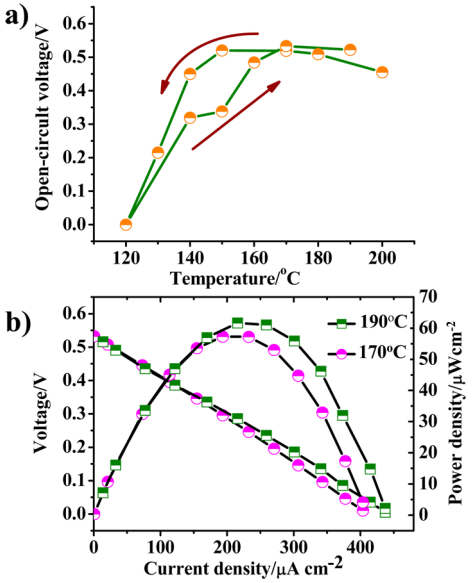

Figure 8. (a) Hysteresis curve of the open circuit voltage as a function of operation temperature: heating (up arrow) and cooling (down arrow) processes. (b) Performance of a single cell under wet hydrogen atmosphere at 170 and 190 °C.

under ambient pressures. The peak power densities of the cell were 62 and 58 uWcm^{-2} at 190 and 170 °C, respectively. The cell performance is too low to be ignored but clearly confirms the potential application of $HNd(IO_3)_4$ as the electrolyte for fuel cells, which can be significantly improved through reducing the cell thickness by choosing proper electrode materials and modifying the cell structure. As shown in Figure 8b, the open-circuit potential of the cell at 170 °C is 0.53 V, which is significantly lower than traditional electrolytes reported before.[21] The OCV is related with the density and electron conductivity of the electrolyte. In addition, $HNd(IO_3)_4$ is an electron isolator (indicated by typical absorption spectra for lanthanide compounds in Figure S8) which avoids internal short circuit to reduce the OCV. Therefore, the electrolyte is possibly not quite dense, which may leak the fuel to further affect the open-circuit potential. However, the OCV can be surely improved by modifying the cell assemble technology in future works. Importantly, we did not observe a noticeable decrease of OCV as a function of cell operating time, which is originated from the chemical and structural robustness possessed by $HNd(IO_3)_4$, clearly demonstrating the promise of a stable protonated 3D inorganic framework material for long-term robust applications in fuel cells.

CONCLUSIONS

A high proton conductivity from room temperature to 553 K was observed in the three-dimensional coordination framework $HNd(IO_3)_4$. Two distinguished conduction mechanisms dominate the proton diffusion process in two separated temperature regions: one is the typically water-mediated conduction below 373 K, and the other is accelerated diffusion along an inherent hydrogen network by thermal activation. Remarkably, the mechanism of this material in high temperature is distinguished with others as it shows no superprotonic phase transition and no dehydration process. Furthermore, $HNd(IO_3)_4$ is facile to be synthesized and exhibits superior chemical and structural robustness at operation conditions. The

DOI: 10.1021/acs.inorgchem.5b01801
Inorg. Chem. 2015, 54, 10023−10029

present work is beneficial to further understanding of the structure−property relationship in proton-conducting materials. As a take-home message of this work, the presented synthesis method under proton-rich environment likely aids in the formation of crystalline materials with liberated protons, which benefits the development of proton-conducting materials.

■ ASSOCIATED CONTENT

Supporting Information

The Supporting Information is available free of charge on the ACS Publications website at DOI: 10.1021/acs.inorgchem.5b01801.

PXRD, materials and characterization, and Nyquist plots (PDF)

X-ray crystallography (CIF)

■ AUTHOR INFORMATION

Corresponding Author

*E-mail: shuaowang@suda.edu.cn.

Author Contributions

‡Y.W., Z.T., and X.Y. contributed equally.

Notes

The authors declare no competing financial interest.

■ ACKNOWLEDGMENTS

We are grateful for funding supported by grants from the National Science Foundation of China (91326112, 21422704), the Science Foundation of Jiangsu Province (BK20140007), a Project Funded by the Priority Academic Program Development of Jiangsu Higher Education Institutions (PAPD), Jiangsu Provincial Key Laboratory of Radiation Medicine and Protection, and "Young Thousand Talented Program" in China. J.S. is thankful for the financial support from the Natural Science Foundation of China (21303111). T.E.A.-S. is supported by the U.S. Department of Energy, Office of Science, Office of Basic Energy Sciences, Heavy Elements Chemistry Program, under Award Number DE-FG02-13ER16414.

■ REFERENCES

(1) (a) Kreuer, K. D. *Chem. Mater.* **1996**, *8*, 610−641. (b) Kreuer, K. D.; Paddison, S. J.; Spohr, E.; Schuster, M. *Chem. Rev.* **2004**, *104*, 4637−4678. (c) Paddison, S. J. *Annu. Rev. Mater. Res.* **2003**, *33*, 289−319.

(2) Li, Q. F.; He, R. H.; Jensen, J. O.; Bjerrum, N. J. *Chem. Mater.* **2003**, *15*, 4896−4915.

(3) (a) Paschos, O.; Kunze, J.; Stimming, U.; Maglia, F. *J. Phys.: Condens. Matter* **2011**, *23*, 234110. (b) Scott, K.; Xu, C. X.; Wu, X. *Wiley Interdiscip. Rev. Energy Environ.* **2014**, *3*, 24−41. (c) Jin, Y.; Shen, Y.; Hibino, T. *J. Mater. Chem.* **2010**, *20*, 6214−6217.

(4) (a) Oono, Y.; Fukuda, T.; Sounai, A.; Hori, M. *J. Power Sources* **2010**, *195*, 1007−1014. (b) Zhang, J.; Tang, Y.; Song, C.; Zhang, J. *J. Power Sources* **2007**, *172*, 163−171.

(5) (a) Haile, S. M.; Boysen, D. A.; Chisholm, C. R. I.; Merle, R. B. *Nature* **2001**, *410*, 910−913. (b) Boysen, D. A.; Uda, T.; Chisholm, C. R. I.; Haile, S. M. *Science* **2004**, *303*, 68−70.

(6) (a) Li, J.-R.; Kuppler, R. J.; Zhou, H.-C. *Chem. Soc. Rev.* **2009**, *38*, 1477−1504. (b) Li, J.-R.; Sculley, J.; Zhou, H.-C. *Chem. Rev.* **2012**, *112*, 869−932. (c) Banerjee, D.; Cairns, A. J.; Liu, J.; Motkuri, R. K.; Nune, S. K.; Fernandez, C. A.; Krishna, R.; Strachan, D. M.; Thallapally, P. K. *Acc. Chem. Res.* **2015**, *48*, 211−219. (d) Zhao, X.; Wong, M.; Mao, C.; Trieu, T. X.; Zhang, J.; Feng, P.; Bu, X. *J. Am. Chem. Soc.* **2014**, *136*, 12572−12575.

(7) (a) Farrusseng, D.; Aguado, S.; Pinel, C. *Angew. Chem., Int. Ed.* **2009**, *48*, 7502−7513. (b) Goesten, M. G.; Juan-Alcaniz, J.; Ramos-Fernandez, E. V.; Gupta, K.; Stavitski, E.; van Bekkum, H.; Gascon, J.; Kapteijn, F. *J. Catal.* **2011**, *281*, 177−187. (c) Laurier, K. G. M.; Vermoortele, F.; Ameloot, R.; De Vos, D. E.; Hofkens, J.; Roeffaers, M. B. J. *J. Am. Chem. Soc.* **2013**, *135*, 14488−14491. (d) Liu, Y.; Xi, X.; Ye, C.; Gong, T.; Yang, Z.; Cui, Y. *Angew. Chem., Int. Ed.* **2014**, *53*, 13821−13825. (e) Yang, D.; Odoh, S. O.; Wang, T. C.; Farha, O. K.; Hupp, J. T.; Cramer, C. J.; Gagliardi, L.; Gates, B. C. *J. Am. Chem. Soc.* **2015**, *137*, 7391−7396.

(8) (a) Harbuzaru, B. V.; Corma, A.; Rey, F.; Jorda, J. L.; Ananias, D.; Carlos, L. D.; Rocha, J. *Angew. Chem., Int. Ed.* **2009**, *48*, 6476−6479. (b) Lu, G.; Hupp, J. T. *J. Am. Chem. Soc.* **2010**, *132*, 7832−7833. (c) Li, Y.; Zhang, S.; Song, D. *Angew. Chem., Int. Ed.* **2013**, *52*, 710−713. (d) Dou, Z.; Yu, J.; Cui, Y.; Yang, Y.; Wang, Z.; Yang, D.; Qian, G. *J. Am. Chem. Soc.* **2014**, *136*, 5527−5530.

(9) Della Rocca, J.; Liu, D. M.; Lin, W. B. *Acc. Chem. Res.* **2011**, *44*, 957−968.

(10) (a) Horike, S.; Umeyama, D.; Kitagawa, S. *Acc. Chem. Res.* **2013**, *46*, 2376−2384. (b) Yamada, T.; Otsubo, K.; Makiura, R.; Kitagawa, H. *Chem. Soc. Rev.* **2013**, *42*, 6655−6669. (c) Yoon, M.; Suh, K.; Natarajan, S.; Kim, K. *Angew. Chem., Int. Ed.* **2013**, *52*, 2688−2700. (d) Ramaswamy, P.; Wong, N. E.; Shimizu, G. K. H. *Chem. Soc. Rev.* **2014**, *43*, 5913−5932.

(11) Shimizu, G. K. H.; Taylor, J. M.; Kim, S. *Science* **2013**, *341*, 354−355.

(12) (a) Yamada, T.; Sadakiyo, M.; Kitagawa, H. *J. Am. Chem. Soc.* **2009**, *131*, 3144−3145. (b) Liang, X.; Zhang, F.; Feng, W.; Zou, X.; Zhao, C.; Na, H.; Liu, C.; Sun, F.; Zhu, G. *Chem. Sci.* **2013**, *4*, 983−992. (c) Sen, S.; Nair, N. N.; Yamada, T.; Kitagawa, H.; Bharadwaj, P. K. *J. Am. Chem. Soc.* **2012**, *134*, 19432−19437. (d) Xu, G.; Yamada, T.; Otsubo, K.; Sakaida, S.; Kitagawa, H. *J. Am. Chem. Soc.* **2012**, *134*, 16524−16527. (e) Xu, G.; Otsubo, K.; Yamada, T.; Sakaida, S.; Kitagawa, H. *J. Am. Chem. Soc.* **2013**, *135*, 7438−7441. (f) Okawa, H.; Sadakiyo, M.; Yamada, T.; Maesato, M.; Ohba, M.; Kitagawa, H. *J. Am. Chem. Soc.* **2013**, *135*, 2256−2262. (g) Bao, S.-S.; Otsubo, K.; Taylor, J. M.; Jiang, Z.; Zheng, L. M.; Kitagawa, H. *J. Am. Chem. Soc.* **2014**, *136*, 9292−9295. (h) Zhai, Q.-G.; Mao, C.; Zhao, X.; Lin, Q.; Bu, F.; Chen, X.; Bu, X.; Feng, P. *Angew. Chem., Int. Ed.* **2015**, *54*, 7886−7890. (i) Phang, W. J.; Lee, W. R.; Yoo, K.; Ryu, D. W.; Kim, B.; Hong, C. S. *Angew. Chem., Int. Ed.* **2014**, *53*, 8383−8387. (j) Nagarkar, S. S.; Unni, S. M.; Sharma, A.; Kurungot, S.; Ghosh, S. K. *Angew. Chem., Int. Ed.* **2014**, *53*, 2638−2642. (k) Phang, W. J.; Jo, H.; Lee, W. R.; Song, J. H.; Yoo, K.; Kim, B.; Hong, C. S. *Angew. Chem., Int. Ed.* **2015**, *54*, 5142−5146. (l) Taylor, J. M.; Mah, R. K.; Moudrakovski, I. L.; Ratcliffe, C. I.; Vaidhyanathan, R.; Shimizu, G. K. H. *J. Am. Chem. Soc.* **2010**, *132*, 14055−14057. (m) Taylor, J. M.; Dawson, K. W.; Shimizu, G. K. H. *J. Am. Chem. Soc.* **2013**, *135*, 1193−1196. (n) Kim, S.; Dawson, K. W.; Gelfand, B. S.; Taylor, J. M.; Shimizu, G. K. H. *J. Am. Chem. Soc.* **2013**, *135*, 963−966. (o) Ramaswamy, P.; Wong, N. E.; Gelfand, B. S.; Shimizu, G. K. H. *J. Am. Chem. Soc.* **2015**, *137*, 7640−7643.

(13) (a) Bureekaew, S.; Horike, S.; Higuchi, M.; Mizuno, M.; Kawamura, T.; Tanaka, D.; Yanai, N.; Kitagawa, S. *Nat. Mater.* **2009**, *8*, 831−836. (b) Umeyama, D.; Horike, S.; Inukai, M.; Hijikata, Y.; Kitagawa, S. *Angew. Chem., Int. Ed.* **2011**, *50*, 11706−11709. (c) Umeyama, D.; Horike, S.; Inukai, M.; Itakura, T.; Kitagawa, S. *J. Am. Chem. Soc.* **2012**, *134*, 12780−12785. (d) Horike, S.; Umeyama, D.; Inukai, M.; Itakura, T.; Kitagawa, S. *J. Am. Chem. Soc.* **2012**, *134*, 7612−7615. (e) Khaletskaya, K.; Reboul, J.; Meilikhov, M.; Nakahama, M.; Diring, S.; Tsujimoto, M.; Isoda, S.; Kim, F.; Kamei, K.-i.; Fischer, R. A.; Kitagawa, S.; Furukawa, S. *J. Am. Chem. Soc.* **2013**, *135*, 10998−11005. (f) Umeyama, D.; Horike, S.; Inukai, M.; Itakura, T.; Kitagawa, S. *J. Am. Chem. Soc.* **2015**, *137*, 864−870. (g) Hurd, J. A.; Vaidhyanathan, R.; Thangadurai, V.; Ratcliffe, C. I.; Moudrakovski, I. L.; Shimizu, G. K. H. *Nat. Chem.* **2009**, *1*, 705−710. (h) Tang, Q.; Liu, Y.; Liu, S.; He, D.; Miao, J.; Wang, X.; Yang, G.; Shi, Z.; Zheng, Z. *J. Am. Chem. Soc.* **2014**, *136*, 12444−12449. (i) Ye, Y.; Zhang, L.; Peng, Q.; Wang, G.-E.; Shen, Y.; Li, Z.; Wang, L.; Ma, X.; Chen, Q.-H.; Zhang, Z.; Xiang, S. *J. Am. Chem. Soc.* **2015**, *137*, 913−918.

DOI: 10.1021/acs.inorgchem.5b01801
Inorg. Chem. 2015, 54, 10023−10029

(14) Sheldrick, G. M. *SHELXTL*; Siemens Analytical X-ray Instruments, Inc.: Madison, WI, 2001.
(15) (a) Feike, M.; Graf, R.; Schnell, I.; Jäger, C.; Spiess, H. *J. Am. Chem. Soc.* **1996**, *118*, 9631−9634. (b) Saalwächter, K.; Lange, F.; Matyjaszewski, K.; Huang, C. F.; Graf, R. *J. Magn. Reson.* **2011**, *212*, 204−215.
(16) (a) Hayashi, S.; Hayamizu, K. B. *Bull. Chem. Soc. Jpn.* **1991**, *64*, 685−687. (b) Morcombe, C. R.; Zilm, K. W. *J. Magn. Reson.* **2003**, *162*, 479−486.
(17) Taouti, M. B.; Gacemi, A.; Benbertal, D.; Gautier-Luneau, I. *Z. Kristallogr. - New Cryst. Struct.* **2008**, *223*, 179−180.
(18) (a) Brese, N. E.; Okeeffe, M. *Acta Crystallogr., Sect. B: Struct. Sci.* **1991**, *47*, 192−197. (b) Urusov, V. S. *Z. Kristallogr. - Cryst. Mater.* **2003**, *218*, 709−719.
(19) (a) Yu, R.; De Jonghe, L. C. *J. Phys. Chem. C* **2007**, *111*, 11003−11007. (b) al-Wahish, A.; Jalarvo, N.; Bi, Z.; Herwig, K. W.; Bridges, C.; Paranthaman, M. P.; Mandrus, D. *J. Phys. Chem. C* **2014**, *118*, 20112−20121.
(20) Haile, S. M.; Chisholm, C. R. I.; Sasaki, K.; Boysen, D. A.; Uda, T. *Faraday Discuss.* **2007**, *134*, 17−39.
(21) (a) Tadanaga, K.; Furukawa, Y.; Hayashi, A.; Tatsumisago, M. *Adv. Mater.* **2010**, *22*, 4401−4404. (b) Song, M.-K.; Li, H.; Li, J.; Zhao, D.; Wang, J.; Liu, M. *Adv. Mater.* **2014**, *26*, 1277−1282.

DOI: 10.1021/acs.inorgchem.5b01801
Inorg. Chem. 2015, 54, 10023−10029